

Article

Stochastic Spatial Binary Simulation with Multivariate Normal Distribution for Illustrating Future Evolution of Umbrella-Shape Summer Shelter under Climate Change

Taesam Lee ^{1,*} , Younghwan Choi ² and Vijay P. Singh ^{3,4}¹ Department of Civil Engineering, Gyeongsang National University, Jinju 52828, Republic of Korea² Urban Design Department, Land and Housing Corporation, Jinju 52852, Republic of Korea³ Department of Biological & Agricultural Engineering, Texas A&M University, College Station, TX 77843-2117, USA⁴ National Water & Energy Center, UAE University, Al Ain 15551, United Arab Emirates

* Correspondence: tae3lee@gnu.ac.kr

Abstract: Surface temperature has increased due to the impact of climate change, and the related weather events, such as heat waves and urban heat island, are occurring more frequently than before. Local governments and planners consider these impacts of climate change and try to avoid them. One of the mainly used structural tools is building summer shelters. A critical issue for urban planners is to test how many shelters should be added and how to distribute the shelters to cope with the impact of climate change. Stochastic simulation models can be a good option to randomize locations of shelters and to see how beneficial for living the shelters can be. Therefore, a novel stochastic simulation model is proposed for distributing summer shelters for coping with the climate change impact. This study proposes a stochastic spatial binary simulation with multivariate normal distribution (SSBM) which contains two major procedures consisting of (1) simulation-based derivation of the empirical function and (2) stochastic simulation of spatial binary data with multivariate normal distribution and the derived empirical function. The proposed model is applied to a case study in Jinju City, South Korea, for the umbrella-shape summer shelters (USS). Results concluded that the proposed SSBM reproduced the statistical characteristics of USS and can be a good alternative to model the locations of USS, including the impact of climate change and investigating the evolution of the USS in the future.

Keywords: climate change; stochastic simulation; summer shelter; spatial distribution; urban



Citation: Lee, T.; Choi, Y.; Singh, V.P. Stochastic Spatial Binary Simulation with Multivariate Normal Distribution for Illustrating Future Evolution of Umbrella-Shape Summer Shelter under Climate Change. *Sustainability* **2023**, *15*, 3147. <https://doi.org/10.3390/su15043147>

Academic Editors: Linchuan Yang, Baojie He and Junqing Tang

Received: 13 December 2022

Revised: 1 February 2023

Accepted: 3 February 2023

Published: 9 February 2023



Copyright: © 2023 by the authors. Licensee MDPI, Basel, Switzerland. This article is an open access article distributed under the terms and conditions of the Creative Commons Attribution (CC BY) license (<https://creativecommons.org/licenses/by/4.0/>).

1. Introduction

Climate change has become a great concern because it affects many natural hazards, such as droughts, floods, and heat waves [1–4]. Heat waves are highly associated with climate change and it is mostly agreed that a substantial increase is projected in the future. South Korea has been reported to be extremely vulnerable in heat waves [5] and their damage is expected to increase in the future [6]. To mitigate the impact of heat waves, summer shelters have been popularly installed. Furthermore, its spatial modeling has been used to assess the usefulness of installed shelters and investigate its spatial evolution due to future climate change [7,8].

Stochastic simulation of spatial and temporal data has been popularly employed to assess the various environmental impacts, including the impact of climate change [9–16]. For example, Delbari, et al. [17] assessed the uncertainty of soil organic carbon affecting many processes in soil with stochastic simulation by generating 100 maps of equiprobable spatial distribution of soil organic carbon. The usefulness and effectiveness of summer shelters to cope with the climate change impact can be assessed through appropriate stochastic simulation with the spatial data for the locations of summer shelters.

Meanwhile, the locations of summer shelters can be categorized as spatial data which can be dealt with binary data [18]. There are three major types of spatial data: geostatistical data, lattice data, and spatial point patterns. Among others, lattice data are counts or spatial averages of a quantity over sub-regions in space, including pixel values from the remote sensing of natural resources (e.g., presence or absence of a plant species in a pixel and population in a county). For example, Tusa, et al. [19] identified the spatial distribution of underweight across Ethiopia. The spatial distribution of underweight was clustered with Global Moran's I. Wang, et al. [20] employed a spatial binary model to illustrate the spatial distribution of fractional vegetation coverage. Likewise, binary spatial modeling has been applied in a number of fields. Khan, et al. [21] employed multivariate binary logistic regression analysis to understand the variables that can explain the hepatitis B vaccination. Locations of the umbrella-shape summer shelters (USS) in a city can be digitized into lattice (binary) data, while the square boundary of a city can be divided to create cells. However, the models reported in the literature are generally used for prediction. The specific purpose of simulation spatial distribution has not been much studied. The spatial diffusion of specific objects such as USS cannot be made with existing models.

Simulating spatial binary data is not direct since the measurement and process of spatial binary data are unique. Therefore, in this current study, a novel stochastic simulation model was proposed to assess the future evolution of USS data, including the impact of climate change. To investigate the future evolution of USS due to the impact of climate change, climate scenarios were employed by correcting the bias in the outputs of climate models. The number of USS in the future was assumed according to the percentage of hot days increasing due to the impact of climate change. The spatial distribution model was devised by employing the spatial autocorrelation structure of USS data as well as the population distribution.

The remainder of this paper is organized as follows. The mathematical background is presented in Section 2, and the proposed method for the stochastic simulation of USS data is presented in Section 3. Section 4 describes the simulation results for the proposed stochastic simulation model. Results of the case study, including climate change impact assessment, is presented in Section 5. Finally, the summary and conclusions are presented in Section 6.

2. Mathematical Background

2.1. Spatial Autocorrelation for Lattice Data

For binary classification, the binary value for the i^{th} cell (Z_i) for $i = 1, \dots, n$ (n is the number of cells) is considered as B (black) or W (white) as in Cressie [18], and is defined as:

$$Z_i = \begin{cases} 1 & \text{if } i^{\text{th}} \text{ pixel is } B \\ 0 & \text{if } i^{\text{th}} \text{ pixel is } W \end{cases} \quad (1)$$

There are three possible joints or couples: BB , BW , and BW . Each joint is defined as:

$$J_{BB} = \frac{1}{2} \sum_{j=1}^n \sum_{i=1}^n \delta_{ij} Z_i Z_j \quad (2)$$

where δ_{ij} is the delta function (i.e., 1 when i^{th} and j^{th} cells are neighbors to each other and 0, otherwise).

$$J_{Bw} = \frac{1}{2} \sum_{j=1}^n \sum_{i=1}^n \delta_{ij} (Z_i - Z_j)^2 \quad (3)$$

$$J_{ww} = A - J_{BB} - J_{BW} \quad (4)$$

where $A = \frac{1}{2} \sum_{j=1}^n \sum_{i=1}^n \delta_{ij}$, i.e., the total number of joints.

Moran's I (denoted as MoI) can be regarded as a correlation coefficient between neighboring Z_i 's [18,22], and can be defined as:

$$I = \frac{n}{2A} \frac{\sum_{j=1}^n \sum_{i=1}^n \delta_{ij} (Z_i - \bar{Z})(Z_j - \bar{Z})}{\sum_{i=1}^n (Z_i - \bar{Z})^2} \quad (5)$$

Note that the delta function (δ_{ij}) can be generalized as a weight (w_{ij}) according to the proximity between cells as:

$$w_{ij} = \frac{\left[\frac{1}{d_{ij}}\right]^\beta}{K} \quad (6)$$

where d_{ij} is the distance between i th and j th cells, β is the parameter (one or two is normally employed) and K is the normalization factor such that $K = \sum_{i=1}^n \left[\frac{1}{d_{ij}}\right]^\beta$. Note that when $\beta = 2$, Equation (6) becomes the inverse distance weight that is commonly employed for interpolation, and this quantity was applied in this current study.

2.2. Multivariate Normal Distribution for Spatial Data

The univariate normal distribution with a mean of μ and variance of σ^2 includes a probability density function (pdf) and cumulative distribution function (cdf), which are expressed [22] as:

$$f(x) = \frac{1}{\sigma\sqrt{2\pi}} \exp\left[-\frac{(x-\mu)^2}{2\sigma^2}\right] \quad (7)$$

$$F(x) = \int_{-\infty}^x \frac{1}{\sigma\sqrt{2\pi}} \exp\left[-\frac{(y-\mu)^2}{2\sigma^2}\right] dy \quad (8)$$

For the standard normal distribution (i.e., $\mu = 0$ and $\sigma^2 = 1$), the pdf has a simpler form as:

$$f(x) = \frac{1}{\sqrt{2\pi}} \exp\left(-\frac{x^2}{2}\right) \quad (9)$$

Additionally, cdf is denoted as $\Phi(x)$. Furthermore, the n -dimensional multivariate normal density of the random vector $\mathbf{X} = [X_1, X_2, \dots, X_n]^T$ is

$$f(x) = \frac{1}{|\boldsymbol{\Sigma}|^{\frac{1}{2}} (2\pi)^n} \exp\left[-(\mathbf{x} - \boldsymbol{\mu})\boldsymbol{\Sigma}^{-1}(\mathbf{x} - \boldsymbol{\mu})/2\right] \quad (10)$$

where $\boldsymbol{\mu}$ represents the $n \times 1$ mean value vector of \mathbf{X} and where $\boldsymbol{\Sigma}$ is the $n \times n$ variance-covariance matrix of \mathbf{X} . The symmetric matrix $\boldsymbol{\Sigma}$ must be positive definite [22]. This density is simply denoted as $MVN_n(\boldsymbol{\mu}, \boldsymbol{\Sigma})$. The covariance and correlation of two variables (X and Y) for $\boldsymbol{\Sigma}$ is defined as:

$$cov(X, Y) = E[(X - EX)(Y - EY)] \quad (11)$$

$$corr(X, Y) = \frac{E[(X - EX)(Y - EY)]}{\sigma_x \sigma_y} \quad (12)$$

In the case of the standard normal distribution for X and Y ,

$$cov(X, Y) = corr(X, Y) = E[XY] \quad (13)$$

Here, $corr(X, Y)$ is a cross-correlation coefficient between cell values. The cross-correlation coefficients among all the grid cells can be denoted by a covariogram, expressed by an exponential function, a modified exponential function, a powered exponential function, or a Gaussian function [23].

In this current study, a powered exponential function was tested due to its popularity. To parameterize the Pearson-based spatial correlation, a powered exponential function is denoted as:

$$\sigma_{ij} = \exp \left[- \left(\frac{d_{ij}}{a} \right) \right] \quad (14)$$

where $\Sigma = [\sigma_{ij}]_{i,j \in [1,m]}$ is the covariance lag-zero matrix and d_{ij} is the distance between the i th and j th grid cells. Additionally, considered as a scale hyperparameter, a is sensitive to the spatial autocorrelation (i.e., MoI). The proposed approach in the following employed the relation between spatial autocorrelation and cross-correlation matrix.

3. Proposed Methodology

The approach proposed in this current study is a stochastic spatial binary simulation with multivariate normal distribution (SSBM), as shown in Figure 1. The SSBM contains two major procedures: (1) the simulation-based parameter derivation procedure using an empirical function (left side of Figure 1) and (2) the stochastic simulation procedure (right side of Figure 1) of spatial binary data with multivariate normal distribution and the derived empirical function. Each procedure is explained separately in the following.

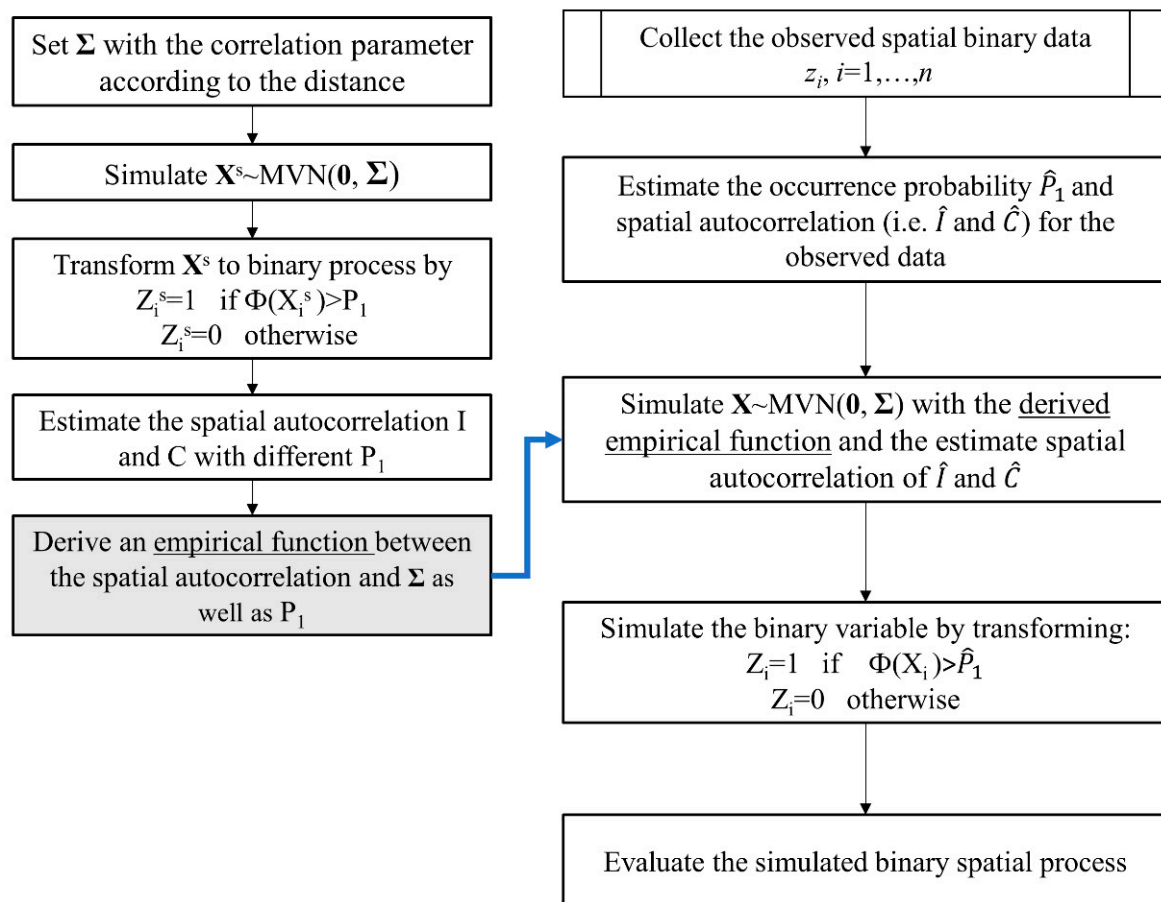


Figure 1. Procedure of the stochastic simulation of the spatial lattice data with the proposed stochastic spatial binary simulation with multivariate normal distribution (SSBM).

3.1. Simulation-Based Derivation Procedure of the Empirical Function

An empirical function associates the relationship between the spatial autocorrelation of MoI as in Equation (5) and the covariance matrix of the multivariate normal distribution presented with the scale hyperparameter of an exponential function as in Equation (14).

- (1) Set the hyperparameters of the covariogram (i.e., a) for the MVN (see Equation (14)).
- (2) Simulate $\mathbf{X}^s \sim \text{MVN}_n(\mathbf{0}, \Sigma)$ with the hyperparameter set from step (1).
- (3) Transform \mathbf{X}^s to binary process \mathbf{Z}^s

$$\begin{cases} Z_i^s = 1 & \text{if } \Phi(X_i^s) > P_1 \\ Z_i^s = 0 & \text{otherwise} \end{cases} \quad (15)$$

where $i = 1, \dots, n$.

- (1) Estimate the spatial autocorrelation MoI (I) with different P_1 from the transformed binary data \mathbf{Z}^s . Note that P_1 indicates the overall probability that $Z_i^s = 1$.
- (2) Derive an empirical function with the relationship between the spatial autocorrelation (i.e., MoI) and the covariance matrix Σ represented with the hyperparameter set. Furthermore, the impact of the occurrence probability P_1 on the spatial autocorrelation must be tested.

3.2. Stochastic Simulation of Spatial Binary Data

- (1) Collect the observed spatial binary data denoted as $z_i, i = 1, \dots, n$.
- (2) Estimate the occurrence probability \hat{P}_1 and spatial autocorrelation (\hat{I}) with the observed data from step (1).
- (3) Simulate multivariate normal variables as $\mathbf{X} \sim \text{MVN}(\mathbf{0}, \Sigma)$ with the hyperparameter set corresponding to the estimated spatial autocorrelation with the observed data (i.e., \hat{I}) using the derived empirical function.
- (4) Transform the simulated multivariate normal variables \mathbf{X} to the spatial binary variables \mathbf{Z} with the estimated occurrence probability \hat{P}_1 in step (1).

4. Simulation Results

4.1. Simulation Methodology

In order to test the performance of the proposed SSBM, a schematic simulation study was conducted. A square gridded area with 140 and 100 pixels in x and y coordinates, respectively, was assumed and the distance between cells was set to be 100 units. Note that the unit can be a meter or a kilometer according to the collected data. The tested parameters of the correlation matrix were $a = [10, 20, 50, 100, 200]$ as in Equation (14), and their magnitudes along with distance are illustrated at the top panel of Figure 2. Note that the correlation is supposed to be weakened as the distance between cells increases, and how fast the correlation dampens substantially belongs to the parameter a as shown in the top panel of Figure 2.

The spatial distribution of the target summer shelter vastly depends on population since higher populated areas require more shelters and vice versa. In this current simulation study, the entire area with 140 and 100 pixels was divided into 4 subsections and the population was set as 500, 2000, 1×10^4 , and 2×10^4 , respectively. The population weight probability was estimated according to the population as:

$$P1_k = Pop_k / \max_{m \in [1, \dots, M]} (Pop_m) \quad (16)$$

where $P1_k$ and Pop_k are the probability and population of the k^{th} subsection, respectively, and M is the number of subsections. In simulation, two probabilities as $P1_k$ in Equation (16) and $\Phi(X_i^s)$ in Equation (15) are equally considered as $P_\Phi = (\Phi(X_i^s) + P1_k)/2$. The probability of $\Phi(X_i^s)$ in Equation (15) in the current simulation is substituted into this combined probability (P_Φ).

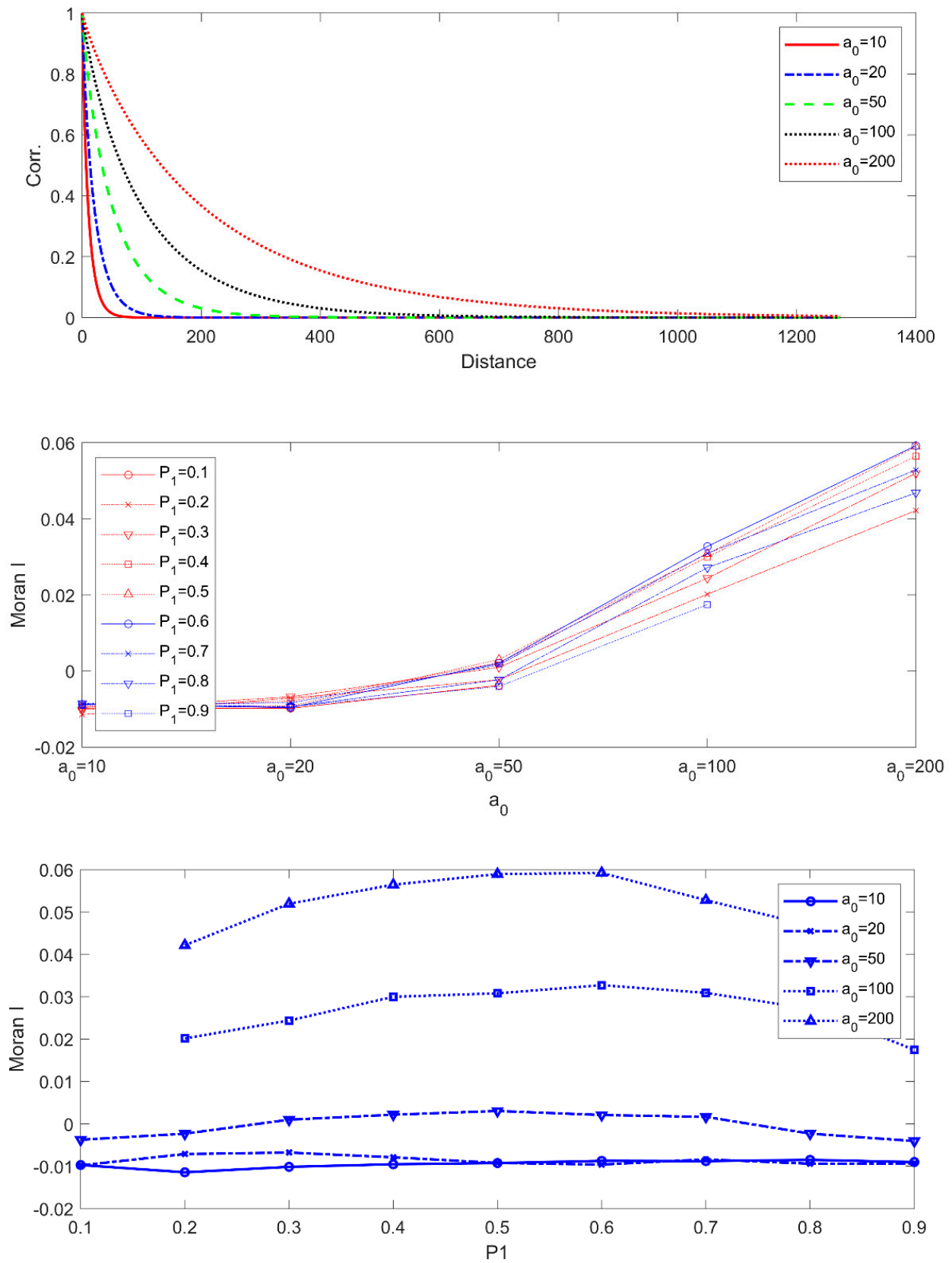


Figure 2. Moran's I along with the occurrence probability of an event at the middle and bottom panels as well as the correlation with distances.

4.2. Simulation Results

The second and third panels of Figure 2 show how the spatial autocorrelation, MoI, for binary lattice data behaves according to the magnitude of the correlation matrix represented with parameter a in Equation (14) and the occurrence probability ($P1$). The second panel of Figure 2 indicates that MoI substantially depends on the correlation structure. In contrast, the occurrence probability ($P1$) seems to slightly affect the MoI spatial autocorrelation as shown in the third panel of Figure 2. Note that the values do not vary along with the $P1$ increase for $a = 10, 20, 50$. In $a = 200$, however, a slight variation can be shown along with $P1$, but seems ignorable. In lower parameter values (i.e., $a = 10, 20$, and 50), MoI did not vary at all, while MoI slightly changed for higher parameter values along with different occurrence probabilities.

For the current simulation, the estimated population probability is presented in Figure 3. As discussed, the entire area was divided into 4 subsections with the maximum probability as one. Note that half of the subsections had a small population probability and the other subsections had 0.5 and 1.0 probability. These population probabilities combined with the simulated probability $\Phi(X_1^s)$ were represented with a correlation matrix and the parameter (i.e., a) that can be estimated with MoI. The region with a higher probability indicated a higher population and vice versa.

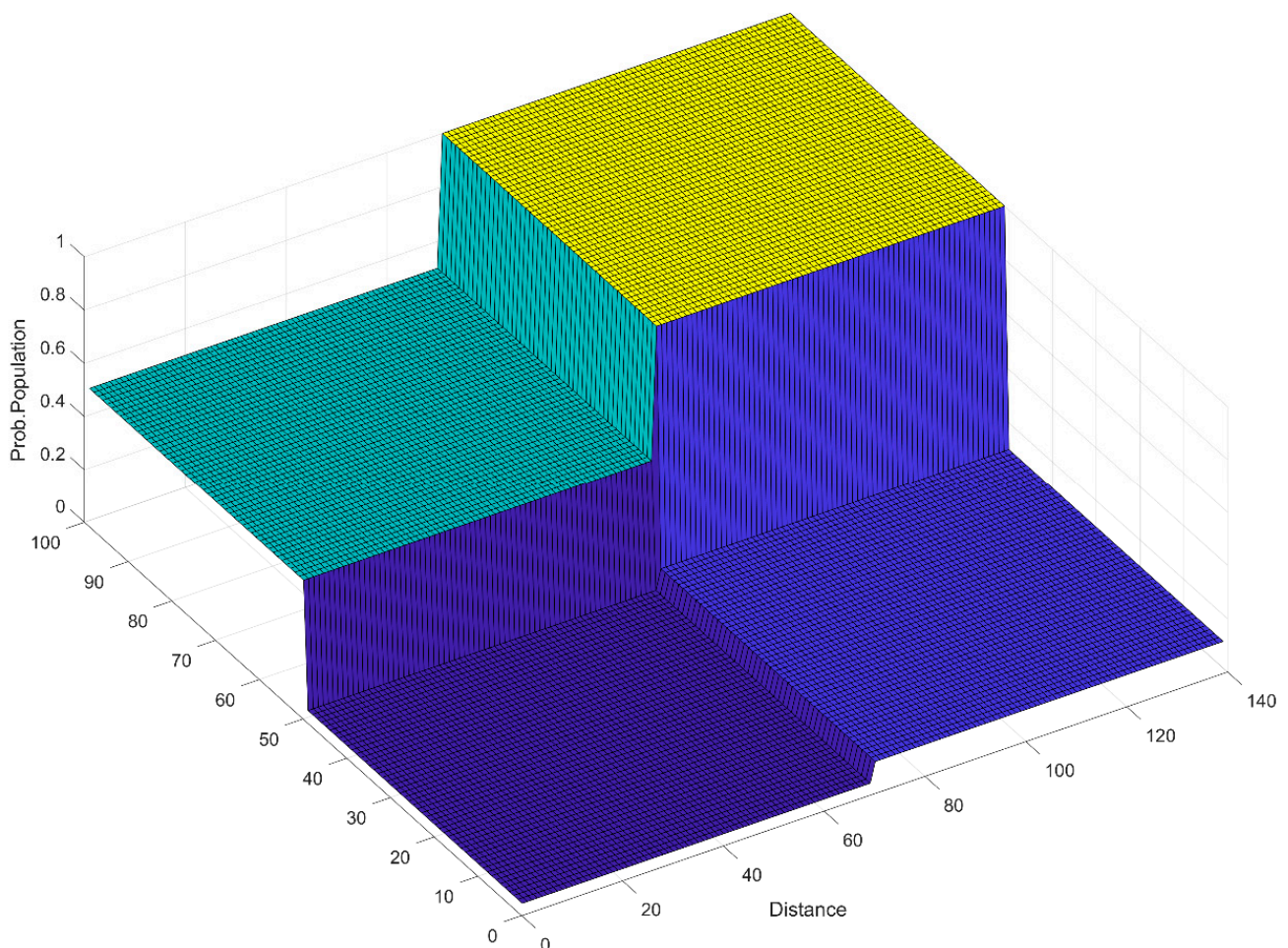


Figure 3. Population probability for testing data. Note that the probability should range from 0.0 to 1.0.

The stochastically simulated data of lattice data was presented in Figure 4 with the initial number of 50 points and increased the number of points as 100, 200, 300, 500, and 1000. With increasing points, new points were generated nearby the existing points. This resulted from the considered spatial autocorrelation of MoI as much as 0.04. Additionally, the density of points was different in each subsection due to the population probability, as shown in Figure 3. The simulation results indicated that the proposed SSBM method reproduced well the intended spatial characteristics.

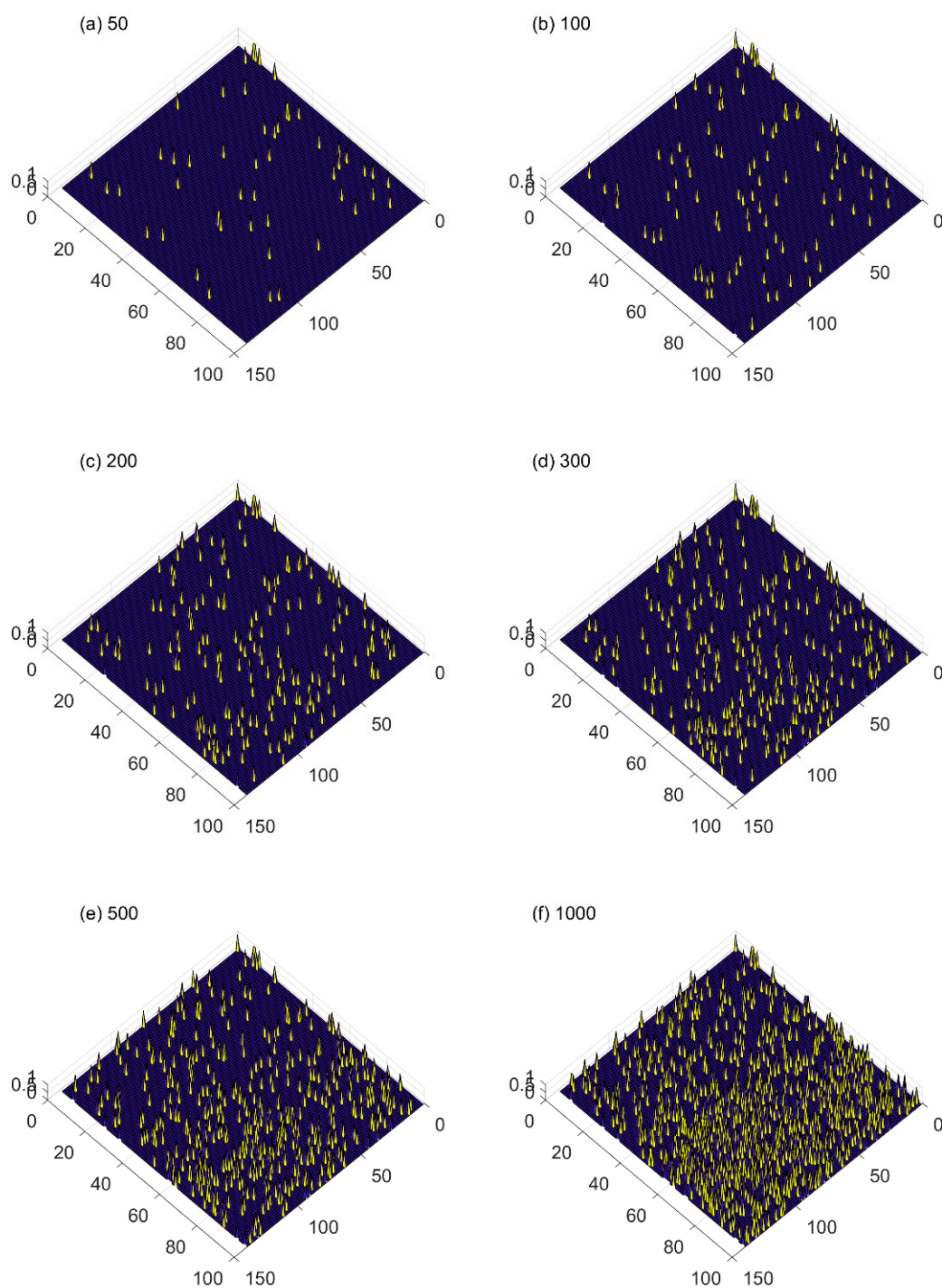


Figure 4. Stochastically simulated data of lattice data with 50 for initial size in panel (a) and increasing the size to 100, 200, 300, 500, 1000 (b–f).

5. Case Study

5.1. Study Area and Data Description

The Jinju area in South Korea was selected as the current study area and was tested in this current study, as shown in Figure 5. The Jinju area is climatologically affected by the Siberian air mass during winter and the Maritime Pacific High during summer. With an average temperature of 25.4 °C, August is the warmest month and January is the coldest month, with temperatures averaging 0.0 °C. In South Korea, summer starts at the end of June and ends in September. The USS data have been collected from the LH as presented in Figure 5, and 120 units have been installed.

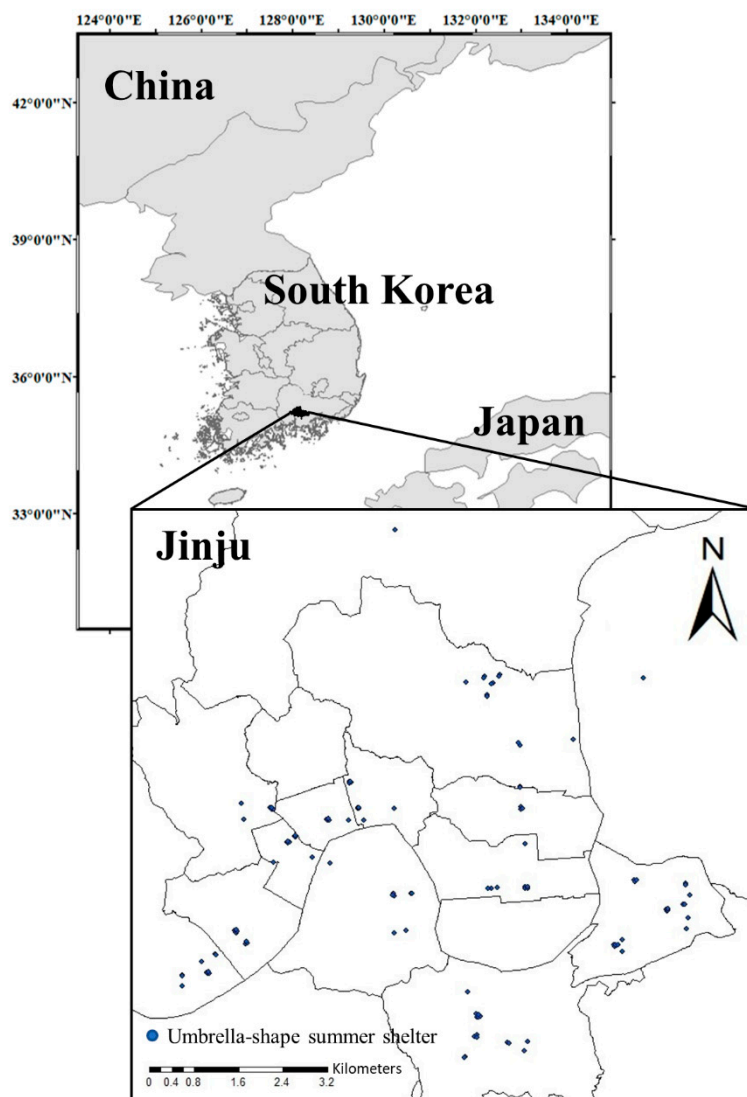


Figure 5. Study area of Jinju, South Korea, and the locations of umbrella-shape summer shelters (USS) shown at the bottom part.

The city of Jinju has been further developed by relocating public sectors and public enterprises, including the Korea Land and Housing Corporation (LH) [24]. Therefore, future population of the city is expected to increase due to the relocation. Meanwhile, the number of heatwave days was found to significantly increase in the recent 20 years compared with the past 1980s and 1990s [25]. Additionally, the duration of heatwave days was projected to increase about two and three times under representative concentration pathway (RCP)4.5 and RCP8.5 climate scenarios [6].

In this current study, it was investigated how the heatwave days were projected with the recent climate projections of shared socioeconomic pathway (SSP) from Earth system models (ESMs) in the Jinju area. To project the future heatwave, 18 ESMs were employed with the SSP245 and SSP585 as well as the base period scenario. The employed ESMs are listed in Table 1 with further information as relative references. The daily temperature data series for the base period and future periods were taken from the gridded ESM data. The closest grid of the ESM data to the Jinju weather station was selected and the corresponding temperature was abstracted.

Table 1. Employed Earth system models (ESMs) and their references.

Institute	Employed ESMs	Reference
Geophysical Fluid Dynamics Laboratory (USA)	GFDL-ESM4	[26]
Meteorological Research Institute (Japan)	MRI-ESM2-0	[27]
Centre National de Recherches Météorologiques (France)	CNRM-CM6-1	[28]
	CNRM-ESM2-1	[29]
Institute Pierre-Simon Laplace (France)	IPSL-CM6A-LR	[30]
Max Planck Institute for Meteorology (Germany)	MPI-ESM1-2-HR	[31]
	MPI-ESM1-2-LR	[32]
Met Office Hadley Centre (UK)	UKESM1-0-LL	[33]
Commonwealth Scientific and Industrial Research Organisation, Australian Research Council Centre of Excellence for Climate System Science (Australia)	ACCESS-CM2	[34]
Commonwealth Scientific and Industrial Research Organisation (Australia)	ACCESS-ESM1-5	[35]
Canadian Centre for Climate Modelling and Analysis (Canada)	CanESM5	[36]
Institute for Numerical Mathematics (Russia)	INM-CM4-8	[28]
	INM-CM5-0	[37]
EC-Earth-Consortium	EC-Earth3	[38]
Japan Agency for Marine-Earth Science and Technology/ Atmosphere and Ocean Research InstituteA/National Institute for Environmental Studies/RIKEN Center for Computational Science (Japan)	MIROC6	[39]
	MIROC-ES2L	[40]
NorESM Climate modeling Consortium consisting of CICERO (Norway)	NorESM2-LM	[41]
National Institute of Meteorological Sciences/Korea Meteorological Administration (Korea)	KACE-1-0-G	[42]

5.2. Applied Methodology

The study area of Jinju was gridded into 50 by 50 cells relative to the size. The SSBM simulation was performed following the procedure in Figure 1. The number of USS was set according to the relative increase of the number of hot days with the future climate scenario. To assess the future evolution of the number of hot days, statistical downscaling was performed with the 18 ESMs. The downscaling results and detailed procedure are explained in the following section.

5.3. Statistical Downscaling Results

Since the daily temperature outputs obtained from the ESMs contain substantial bias compared to observations, a number of bias-correction models have been suggested, such as quantile mapping, detrended quantile mapping, and quantile delta mapping [43]. Quantile delta mapping (QDM) was applied in this current study, since QDM did not inflate much the magnitude of relative trend projected by climate models [44], and it preserved better the change signal for temperature in summer [45].

The exceedance probabilities (ExPr) of daily maximum temperature (DMT) for observed and SSP scenarios are presented in Figure 6. Note that (1) the ESMorg indicating the ExPr of the base period for the climate scenario overlapped with the observed data, as shown in the top panel of Figure 6, and (2) the ESMorg data of the base period further moved to the right side indicating that the temperature high values of the ESMorg data were underestimated and adjusted to the observed data. The temperature values of the future SSP45 and SSP85 scenarios had been bias-corrected and were presented with the light blue solid line and cross marker shown in the second and bottom panel of Figure 6. The results presented that the future high temperature values were higher than the observed data, representing that the extreme temperatures of the future scenarios were expected to increase according to SSP245 and SSP285. Additionally, it showed the temperature with the SSP285 scenario increased up to 45 °C, while the one with SSP245 was about 41 °C. This implied that the hot days of the Jinju area were more significant in the future and the SSP285 scenario showed a higher magnitude than did SSP245.

The number of hot days (HDs) was estimated for SSP245 and SSP285 scenarios with the bias-corrected temperature for the current period and the future period, as shown in Figure 7, and its average is presented in Table 2. Note that a hot day was defined as a daily maximum temperature ≥ 33 °C [46]. The future years were divided into three periods as P1: 2015–2040, P2: 2041–2070, and P3: 2071–2100, while the base period and observed years were set to be 1979–2014. It was noted that the number of hot days increased up to 4.9-fold and 8.6-fold with the SSP245 and SSP285 scenarios, respectively, relative to the base period and the observed data. It was expected that the requirement of USS might increase due to the substantial increase of HDs according to the future temperature. Therefore, it was assumed that the USS increased at the same rate of HD in the future, and the estimated future USS was presented on the right side of Table 2. The results showed that the number of USS increased up to 200 in the P1 period with both SSP245 and 285 scenarios and in the P3 period, it increased up to about 600 and 1000.

Table 2. Projected hot days and number of umbrella-shape summer shelters (USS).

Time	No. of HD		Relative HD (%) *		Future No. of USS †	
	SSP245	SSP285	SSP245	SSP285	SSP245	SSP285
Obs	7.92		100.00		120	
Base	7.90		99.83		120	
P1	13.04	13.02	164.70	164.52	198	197
P2	26.54	33.86	335.29	427.72	402	513
P3	38.72	68.57	489.15	866.19	587	1039

* Relative hot days (HD) were estimated with the number of USS for the current and future period divided by the number of HDs in observation. † Future number of USS was calculated with the number of USS multiplied by the relative HD.

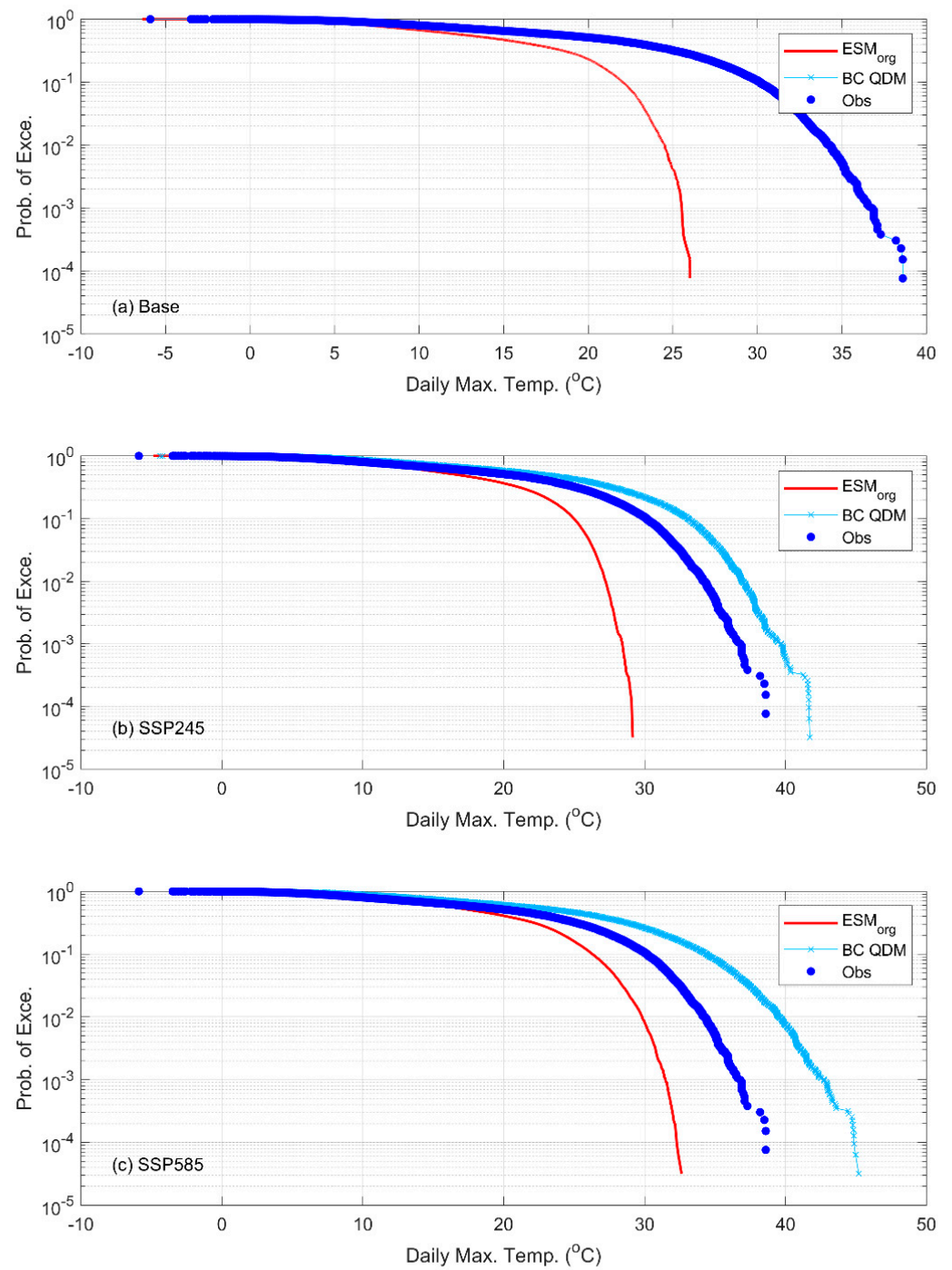


Figure 6. Exceedance probability of daily maximum temperature for the observed data (blue dots) and SSP245 (top panel), and 285 (bottom panel) scenarios of the original ESM outputs (red solid line) and the bias-corrected quantile delta mapping (BC QDM, dotted line with x marker).

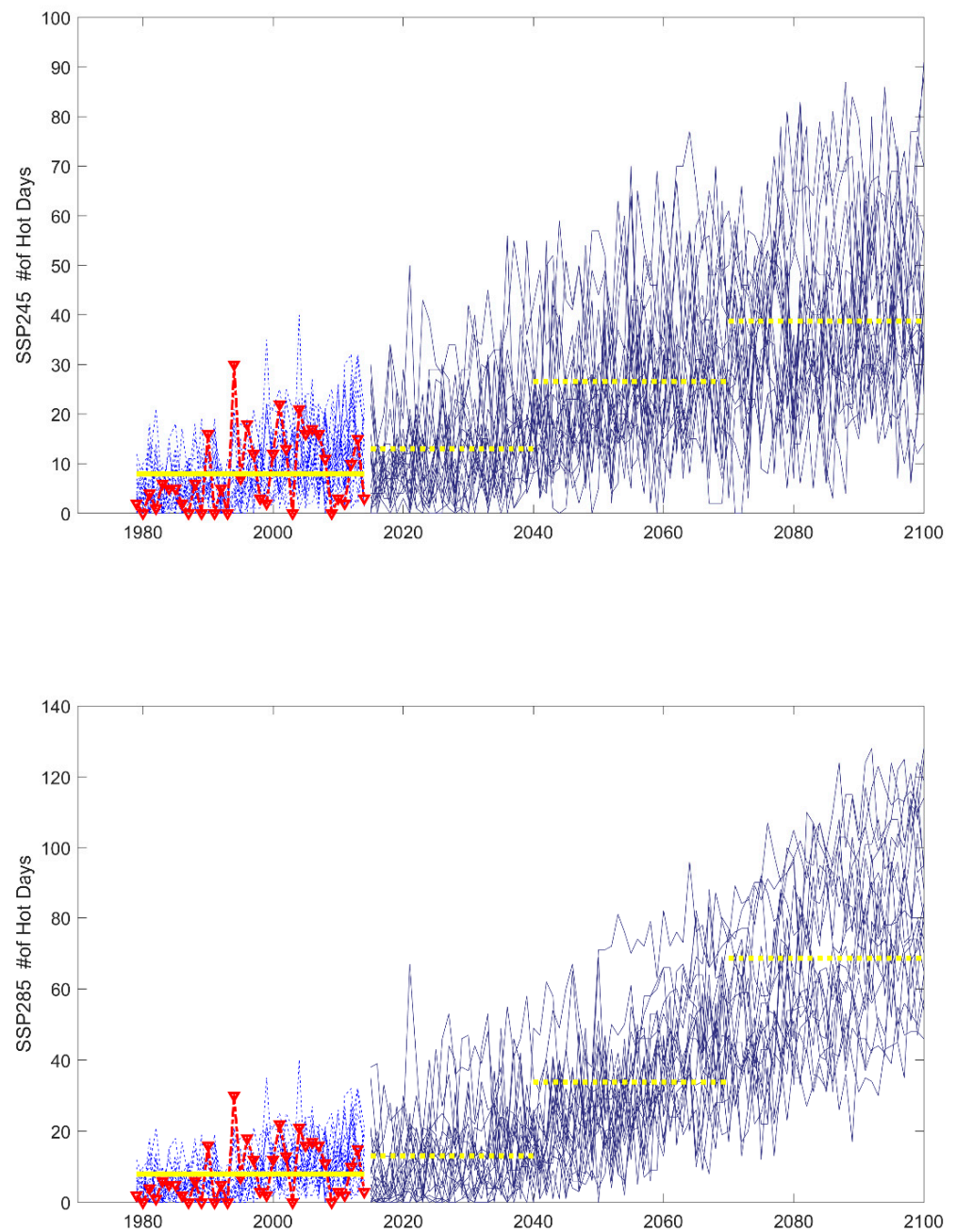


Figure 7. Number of hot days for the current and future climate SSP245 (**top panel**) and SSP285 (**bottom panel**) scenarios with 25 ESModel models. The red and blue lines indicate the observation data and the ESModel data for the base period, while the yellow line presents the periodic average for 30 years as P1: 2015–2040, P2: 2041–2070, and P3: 2071–2100, and the base period and observed years are set to be 1979–2014.

5.4. Stochastic Simulation of Umbrella-Shape Summer Shelter (USS)

The population probability was estimated, as shown in Figure 8. The density of the Jinju population was highly localized since the city was separated into urban and rural areas. Also, the density of the USS location presented a similar pattern to the population.

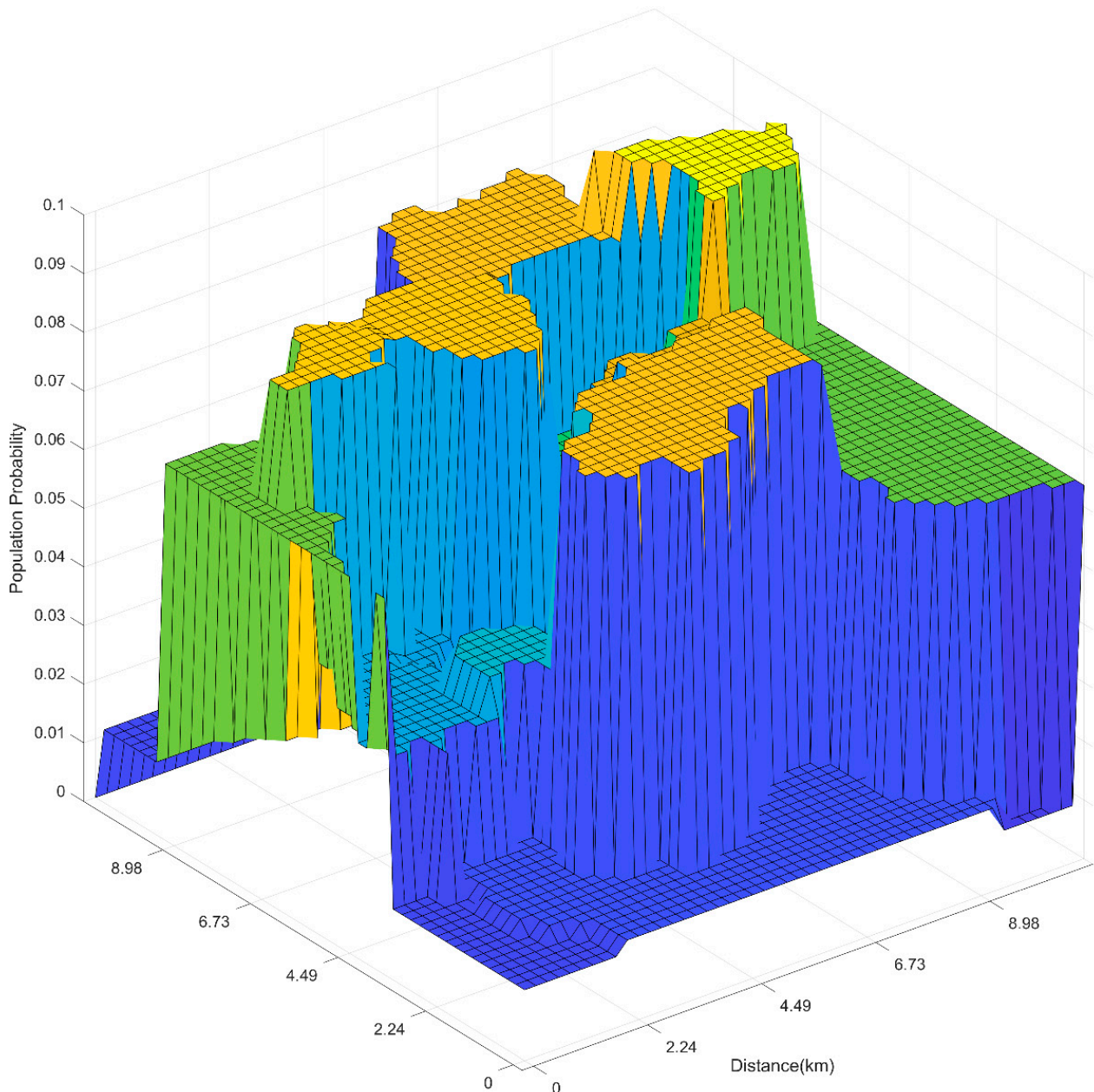


Figure 8. Population probability over Jinju area for distances.

Since the target number of the future USS was assumed, the related parameter for the SSBM model was estimated, as suggested (see Figure 1). The MoI was estimated with the USS data in Jinju, as shown in Figure 5, with the gridded 50 by 50 cells, and the estimated MoI was 0.0455. Parameter, a , of the correlation matrix in Equation (14) was estimated with the simulation-based empirical relation, as shown in Figure 9. The bottom panel showed that the closest parameter with MoI ($= 0.0455$) was 1.2. Subsequently, the parameter (i.e., $a = 1.2$) was applied in simulation.

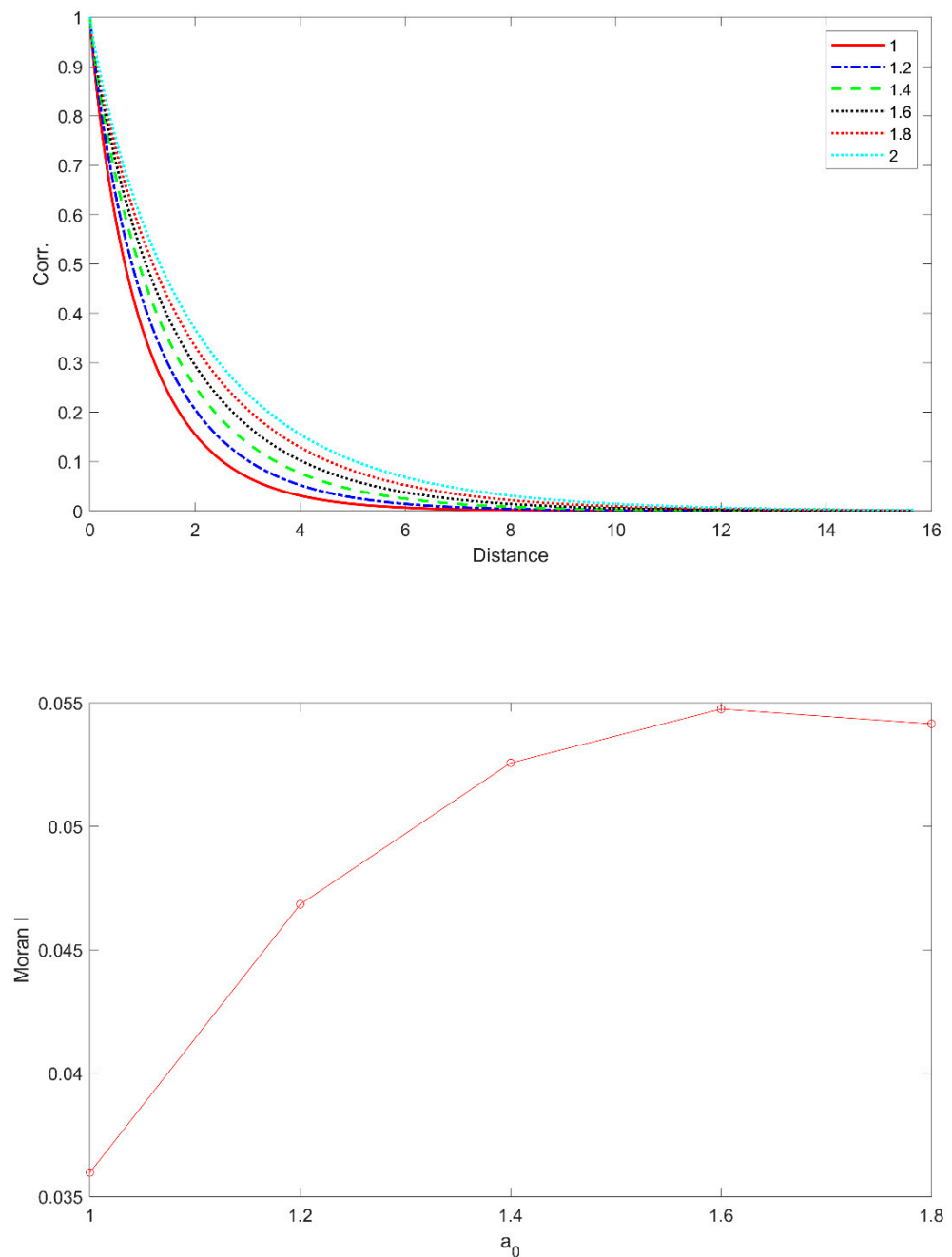


Figure 9. Correlation of M_0 with different scale parameters (i.e., a in Equation (14), top panel) and Moran's I (bottom panel) with the occurrence probability of the observed USS data in Jinju.

With the estimated parameter for the SSBM model and the population probability, as well as the future projection of the number of USS, the future spatial distribution was simulated, as shown in Figure 10. The initial locations of the USS showed that they were rather clustered, indicating substantial spatial autocorrelation up to 0.0455 MoI, and it was evident that the population highly affected the locations of the USS in Jinju. The sporadic distribution of the USS showed the stochastic characteristics of USS. As the USS value increased, the area with the USS increased and the clusters weakened. The new locations of USS were close to the existing units and also new USS, apart from the existing ones, were also located due to the stochastic nature of the SSBM model.

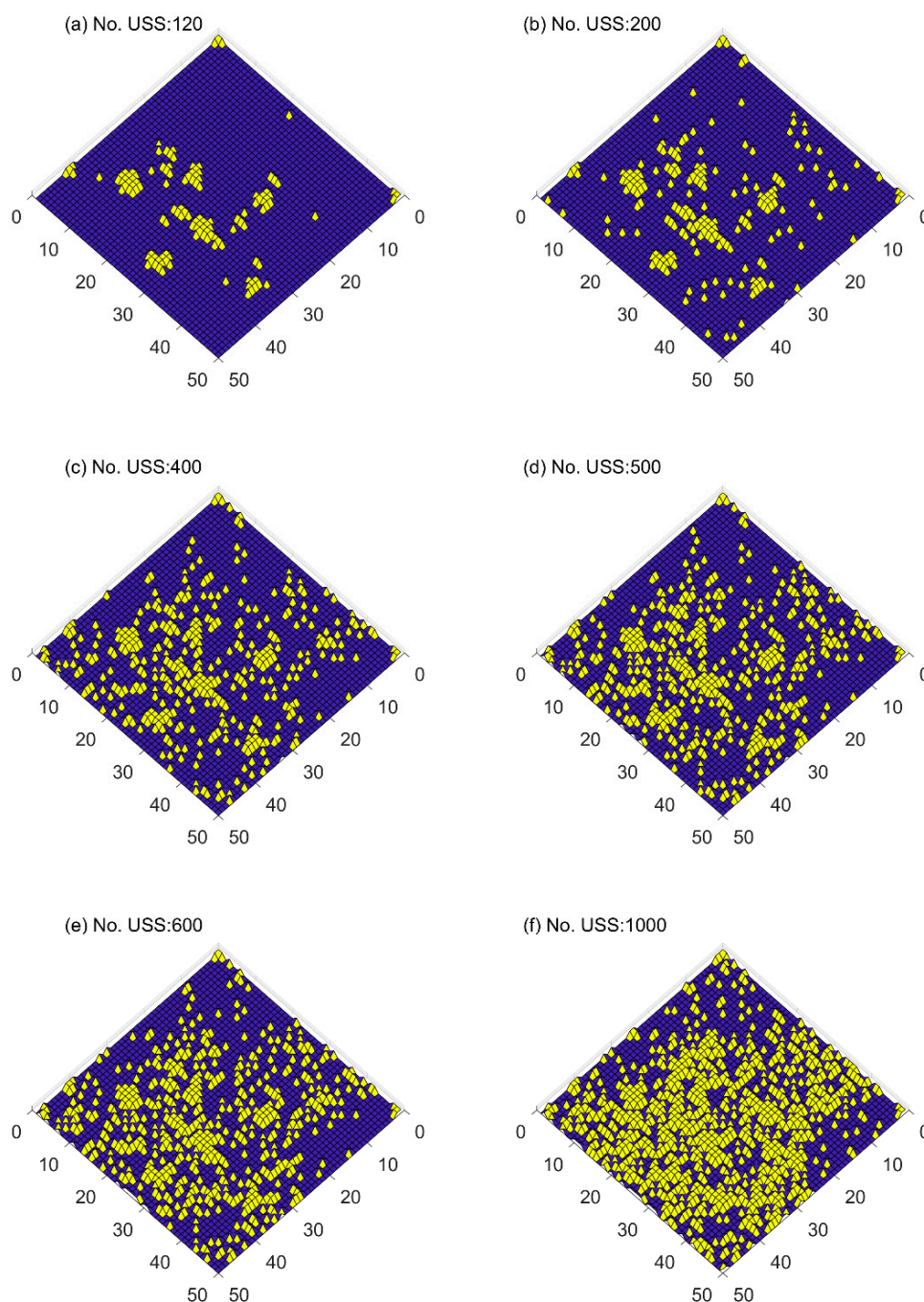


Figure 10. Spatial stochastic simulation of the binary process for USS in Jinju with adding 100, 200, and 600 for the future projection as in Table 2.

6. Summary and Conclusions

This current study proposed a novel stochastic simulation model for spatial binary lattice data, called as SSBM, to model the spatial revolution of binary spatial data, such as USS. The SSBM model employed the spatial autocorrelation of MoI to estimate the correlation matrix represented with the scale parameter. The proposed model was tested in a simulation study, including a nonhomogeneous population. The simulation result indicated that the proposed SSBM model reproduced well the spatial binary characteristics.

Furthermore, the proposed SSBM model was applied to show the future evolution of the USS data, which was spatial binary lattice data in Jinju. To conjecture the future number of USS, the number of hot days with climate scenarios were projected with SSP245 and SSP285 scenarios with 18 ESMs. The future projection results showed that hot days might increase 5- and 8-fold according to the SSP245 and SSP285 scenarios, respectively. Therefore, the number of USS was assumed to increase 5- and 8-fold as 600 and 1000 units. The case study results of the USS data in the future indicated that the proposed SSBM model reproduced well the future evolution of the USS spatial binary data. The proposed model can be extended to apply any spatial binary data and is useful to assess how spatial binary data can be distributed according to climate scenarios.

The SSBM model proposed in this current study is also applicable to any part of the world as long as the current USS location map and future climate condition are obtained. Furthermore, the proposed SSBM model can be employed to derive the spatial divergence of any particular objects, such as diseases and insects. Model improvements can be made to adopt exogeneous variables. This modification can be easily made by extending the MVB distribution as conditional MVN [16]. Alternatively, binary logistic model can be tested instead of the SSBM, even though a mathematical development to apply the USS data has not yet occurred [21].

Author Contributions: Conceptualization, T.L. and Y.C.; methodology, V.P.S.; software, T.L.; validation, T.L. and V.P.S.; formal analysis, Y.C.; investigation, T.L.; resources, Y.C.; data curation, Y.C.; writing—original draft preparation, T.L. and Y.C.; writing—review and editing, T.L. and V.P.S.; visualization, T.L.; supervision, V.P.S.; project administration, Y.C.; funding acquisition, T.L. All authors have read and agreed to the published version of the manuscript.

Funding: This work was supported by the National Research Foundation of Korea (NRF) grant funded by the Korean Government (MEST). The first author also acknowledges that this research was partially supported by a grant (2022-MOIS63–001) of Cooperative Research Method and Safety Management Technology in National Disaster funded by Ministry of Interior and Safety (MOIS, Korea).

Informed Consent Statement: Not applicable.

Data Availability Statement: The data that support the findings of this study are available from the corresponding author, T. Lee, upon reasonable request.

Conflicts of Interest: The authors declare no conflict of interest.

References

1. Son, C.; Lee, T.; Kim, M.; Lee, S.; Yoon, S. Climate Change Adaptation to Extreme Rainfall Events on a Local Scale in Namyangju, South Korea. *J. Hydrol. Eng.* **2020**, *25*, 05020005.
2. Díaz, J.; Linares, C.; Tobías, A. Impact of extreme temperatures on daily mortality in Madrid (Spain) among the 45–64 age-group. *Int. J. Biometeorol.* **2006**, *50*, 342–348. [[PubMed](#)]
3. Laaidi, M.; Laaidi, K.; Besancenot, J.P. Temperature-related mortality in France, a comparison between regions with different climates from the perspective of global warming. *Int. J. Biometeorol.* **2006**, *51*, 145–153.
4. Takahashi, K.; Honda, Y.; Emori, S. Assessing mortality risk from heat stress due to global warming. *J. Risk Res.* **2007**, *10*, 339–354.
5. Kyselý, J.; Kim, J. Mortality during heat waves in South Korea, 1991 to 2005: How exceptional was the 1994 heat wave? *Clim. Res.* **2009**, *38*, 105–116.
6. Kim, D.-W.; Deo, R.C.; Chung, J.-H.; Lee, J.-S. Projection of heat wave mortality related to climate change in Korea. *Nat. Hazards* **2016**, *80*, 623–637.
7. Kosatsky, T.; Dufresne, J.; Richard, L.; Renouf, A.; Giannetti, N.; Bourbeau, J.; Julien, M.; Braid, T.; Sauve, C. Heat awareness and response among Montreal residents with chronic cardiac and pulmonary disease. *Can. J. Public Health* **2009**, *100*, 237–240. [[CrossRef](#)]
8. Joon, V.; Jaiswal, V. Impact of climate change on human health in India: An overview. *Health Popul. Perspect. Issues* **2012**, *35*, 11–22.
9. Malek, Ž.; Verburg, P.H. Representing responses to climate change in spatial land system models. *Land Degrad. Dev.* **2021**, *32*, 4954–4973. [[CrossRef](#)]
10. Bhattacharya, S. A simulation approach to Bayesian emulation of complex dynamic computer models. *Bayesian Anal.* **2007**, *2*, 783–816. [[CrossRef](#)]

11. Dunn, S.M.; Johnston, L.; Taylor, C.; Watson, H.; Cook, Y.; Langan, S.J. Capability and limitations of a simple grid-based model for simulating land use influences on stream nitrate concentrations. *J. Hydrol.* **2013**, *507*, 110–123.
12. Wang, D.; Wu, J.; Huang, M.; Li, L.Z.X.; Wang, D.; Lin, T.; Dong, L.; Li, Q.; Yang, L.; Zeng, Z. The Critical Effect of Subgrid-Scale Scheme on Simulating the Climate Impacts of Deforestation. *J. Geophys. Res. Atmos.* **2021**, *126*, e2021JD035133.
13. Lee, T.S. Stochastic Simulation of Hydrologic Data Based on Nonparametric Approaches. Ph.D. Dissertation, Colorado State University, Fort Collins, CO, USA, 2008.
14. Lee, T. Multisite stochastic simulation of daily precipitation from copula modeling with a gamma marginal distribution. *Theor. Appl. Climatol.* **2018**, *132*, 1089–1098.
15. Lee, T.; Ouarda, T.B.M.J. Multivariate Nonstationary Oscillation Simulation of Climate Indices with Empirical Mode Decomposition. *Water Resour. Res.* **2019**, *55*, 5033–5052.
16. Lee, T.; Ouarda, T.B.M.J. Conditional stochastic simulation model for spatial downscaling for assessing the effects of climate change on hydro-meteorological variables. *Clim. Chang.* **2018**, *150*, 163–180. [[CrossRef](#)]
17. Delbari, M.; Loiskandl, W.; Afrasiab, P. Uncertainty assessment of soil organic carbon content spatial distribution using geostatistical stochastic simulation. *Aust. J. Soil Res.* **2010**, *48*, 27–35.
18. Cressie, N.A.C. *Statistics for Spatial Data*; John Wiley & Sons, Inc.: New York, NY, USA, 1993; p. 900.
19. Tusa, B.S.; Weldesenbet, A.B.; Kebede, S.A. Spatial distribution and associated factors of underweight in Ethiopia: An analysis of Ethiopian demographic and health survey, 2016. *PLoS ONE* **2020**, *15*, e0242744. [[CrossRef](#)]
20. Wang, R.; Yan, F.; Wang, Y. Vegetation growth status and topographic effects in the pisha sandstone area of China. *Remote Sens.* **2020**, *12*, 2759.
21. Khan, J.; Shil, A.; Mohanty, S.K. Hepatitis B vaccination coverage across India: Exploring the spatial heterogeneity and contextual determinants. *BMC Public Health* **2019**, *19*, 1263. [[CrossRef](#)]
22. Johnson, R.A.; Wichern, D.W. *Applied Multivariate Statistical Analysis*; Prentice Hall: Upper Saddle River, NJ, USA, 2001; p. 767.
23. Zimmerman, D.L. *Spatial Design, Optimal*; John Wiley & Sons, Ltd.: New York, NY, USA, 2014.
24. Kim, W.Y.; Kim, M.K.K. The Effects of Public Sector Relocation on Population and Employment: The Case of Jinju City. *J. Korean Assoc. Reg. Geogr.* **2021**, *27*, 144–163.
25. Yoon, D.; Cha, D.-H.; Lee, M.-I.; Min, K.-H.; Kim, J.; Jun, S.-Y.; Choi, Y. Recent changes in heatwave characteristics over Korea. *Clim. Dyn.* **2020**, *55*, 1685–1696.
26. John, J.G.; Blanton, C.; McHugh, C.; Radhakrishnan, A.; Rand, K.; Vahlenkamp, H.; Wilson, C.; Zadeh, N.T.; Dunne, J.P.; Dussin, R.; et al. NOAA-GFDL GFDL-ESM4 model output prepared for CMIP6 ScenarioMIP. In *Earth System Grid Federation*; Pearson Education Limited: London, UK, 2018.
27. Yukimoto, S.; Koshiro, T.; Kawai, H.; Oshima, N.; Yoshida, K.; Urakawa, S.; Tsujino, H.; Deushi, M.; Tanaka, T.; Hosaka, M.; et al. MRI MRI-ESM2.0 model output prepared for CMIP6 ScenarioMIP. In *Earth System Grid Federation*; Pearson Education Limited: London, UK, 2019.
28. Voldoire, A. CNRM-CERFACS CNRM-CM6-1 model output prepared for CMIP6 ScenarioMIP. In *Earth System Grid Federation*; Pearson Education Limited: London, UK, 2019.
29. Seferian, R. CNRM-CERFACS CNRM-ESM2-1 model output prepared for CMIP6 ScenarioMIP. In *Earth System Grid Federation*; Pearson Education Limited: London, UK, 2019.
30. Boucher, O.; Denvil, S.; Levavasseur, G.; Cozic, A.; Caubel, A.; Foujols, M.-A.; Meurdesoif, Y.; Cadule, P.; Devilliers, M.; Dupont, E.; et al. IPSL IPSL-CM6A-LR model output prepared for CMIP6 ScenarioMIP. In *Earth System Grid Federation*; Pearson Education Limited: London, UK, 2019.
31. Gutzjahr, O.; Putrasahan, D.; Lohmann, K.; Jungclaus, J.H.; Von Storch, J.S.; Brüggemann, N.; Haak, H.; Stössel, A. Max Planck Institute Earth System Model (MPI-ESM1.2) for the High-Resolution Model Intercomparison Project (HighResMIP). *Geosci. Model Dev.* **2019**, *12*, 3241–3281.
32. Wieners, K.-H.; Giorgetta, M.; Jungclaus, J.; Reick, C.; Esch, M.; Bittner, M.; Gayler, V.; Haak, H.; de Vrese, P.; Raddatz, T.; et al. MPI-M MPIESM1.2-LR model output prepared for CMIP6 ScenarioMIP. In *Earth System Grid Federation*; Pearson Education Limited: London, UK, 2019.
33. Good, P.; Sellar, A.; Tang, Y.; Rumbold, S.; Ellis, R.; Kelley, D.; Kuhlbrodt, T.; Walton, J. MOHC UKESM1.0-LL model output prepared for CMIP6 ScenarioMIP. In *Earth System Grid Federation*; Pearson Education Limited: London, UK, 2019.
34. Dix, M.; Bi, D.; Dobrohotoff, P.; Fiedler, R.; Harman, I.; Law, R.; Mackallah, C.; Marsland, S.; O'Farrell, S.; Rashid, H.; et al. CSIRO-ARCCSS ACCESS-CM2 model output prepared for CMIP6 ScenarioMIP. In *Earth System Grid Federation*; Pearson Education Limited: London, UK, 2019.
35. Ziehn, T.; Chamberlain, M.; Lenton, A.; Law, R.; Bodman, R.; Dix, M.; Wang, Y.; Dobrohotoff, P.; Srbinovsky, J.; Stevens, L.; et al. CSIRO ACCESS-ESM1.5 model output prepared for CMIP6 ScenarioMIP. In *Earth System Grid Federation*; Pearson Education Limited: London, UK, 2019.
36. Swart, N.C.; Cole, J.N.S.; Kharin, V.V.; Lazare, M.; Scinocca, J.F.; Gillett, N.P.; Anstey, J.; Arora, V.; Christian, J.R.; Jiao, Y.; et al. CCCma CanESM5 model output prepared for CMIP6 ScenarioMIP. In *Earth System Grid Federation*; Pearson Education Limited: London, UK, 2019.

37. Volodin, E.; Mortikov, E.; Gritsun, A.; Lykossov, V.; Galin, V.; Diansky, N.; Gusev, A.; Kostykin, S.; Iakovlev, N.; Shestakova, A.; et al. INM INM-CM4-8 model output prepared for CMIP6 ScenarioMIP. In *Earth System Grid Federation*; Pearson Education Limited: London, UK, 2019.
38. Consortium, E.C.E. EC-Earth-Consortium EC-Earth3 model output prepared for CMIP6 ScenarioMIP. In *Earth System Grid Federation*; Pearson Education Limited: London, UK, 2019.
39. Shiogama, H.; Abe, M.; Tatebe, H. MIROC MIROC6 model output prepared for CMIP6 ScenarioMIP. In *Earth System Grid Federation*; Pearson Education Limited: London, UK, 2019.
40. Tachiiri, K.; Abe, M.; Hajima, T.; Arakawa, O.; Suzuki, T.; Komuro, Y.; Ogochi, K.; Watanabe, M.; Yamamoto, A.; Tatebe, H.; et al. MIROC MIROC-ES2L model output prepared for CMIP6 ScenarioMIP. In *Earth System Grid Federation*; Pearson Education Limited: London, UK, 2019.
41. Seland, Ø.; Bentsen, M.; Olivieri, D.J.L.; Toniazzo, T.; Gjermundsen, A.; Graff, L.S.; Debernard, J.B.; Gupta, A.K.; He, Y.; Kirkevåg, A.; et al. NCC NorESM2-LM model output prepared for CMIP6 ScenarioMIP. In *Earth System Grid Federation*; Pearson Education Limited: London, UK, 2019.
42. Byun, Y.-H.; Lim, Y.-J.; Sung, H.M.; Kim, J.; Sun, M.; Kim, B.-H. NIMS-KMA KACE1.0-G model output prepared for CMIP6 CMIP amip. In *Earth System Grid Federation*; Pearson Education Limited: London, UK, 2019.
43. Lee, T.; Singh, V.P. *Statistical Downscaling for Hydrological and Environmental Applications*; CRC Press: Boca Raton, FL, USA, 2018; Volume 1, p. 181.
44. Cannon, A.J.; Sobie, S.R.; Murdock, T.Q. Bias correction of GCM precipitation by quantile mapping: How well do methods preserve changes in quantiles and extremes? *J. Clim.* **2015**, *28*, 6938–6959. [[CrossRef](#)]
45. Tong, Y.; Gao, X.; Han, Z.; Xu, Y.; Xu, Y.; Giorgi, F. Bias correction of temperature and precipitation over China for RCM simulations using the QM and QDM methods. *Clim. Dyn.* **2021**, *57*, 1425–1443. [[CrossRef](#)]
46. Koo, Y.; Kim, J.; Kim, J.; Lee, S. Study on the Improvement of Adaptation Ability by Vulnerability Analysis of Heat Wave—The Case of Busan Metropolitan City. *Korean Reg. Dev. Assoc.* **2015**, *27*, 331–347.

Disclaimer/Publisher’s Note: The statements, opinions and data contained in all publications are solely those of the individual author(s) and contributor(s) and not of MDPI and/or the editor(s). MDPI and/or the editor(s) disclaim responsibility for any injury to people or property resulting from any ideas, methods, instructions or products referred to in the content.